

The sources of extended continuum emission towards Q0151+048A : The host galaxy and the Damped Ly α Absorber ^{*}

J.U. Fynbo^{1,2}, I. Burud³, and Palle Møller²

¹ Institute of Physics and Astronomy, University of Århus, DK-8000 Århus C, Denmark

² European Southern Observatory, Karl-Schwarzschild-Straße 2, D-85748, Garching by München, Germany

³ Institut d'Astrophysique et de Geophysique de Liège, Université de Liège, Avenue de Cointe 5, B-4000 Liège, Belgium

Received ; accepted

Abstract. We present deep imaging in the U, B and I bands obtained under excellent seeing conditions of the double quasar Q0151+048A,B and of the Damped Ly α (DLA) absorbing galaxy at $z_{\text{abs}} = 1.9342$ named S4.

We analyse the data employing two separate and independent methods. First we deconvolve the images using the MCS algorithm, secondly we decompose the images via an object based iteration process where we fit models to objects without any attempt to improve the resolution of the data. Our detailed analysis of the images reveals, somewhat surprisingly, that extended objects centred on the quasars themselves are much brighter continuum sources than the DLA galaxy.

Due to the complexity caused by the many superimposed objects, we are unable to certify whether or not continuum emission from the DLA galaxy is detected. Continuum emission from the extended objects centred on the positions of the quasars is clearly seen, and the objects are tentatively identified as the “host galaxies” of the quasars. The flux of those host galaxies is of order 2–6% of the quasar flux, and the light profile of the brighter of the two is clearly best fit with a de Vaucouleurs profile. We discuss two alternative interpretations of the origin of the extended flux: *i*) the early stage of a massive elliptical galaxy in the process of forming the bulk of its stars, and *ii*) quasar light scattered by dust.

Key words: quasars : absorption lines – quasars : Q0151+048 – galaxies : intergalactic medium – galaxies : photometry – methods : data analysis

1. Introduction

The study of the galaxy population at high redshifts has progressed rapidly during the last decade. Through the Lyman-break technique hundreds of normal (i.e. not dominated by ac-

tive galactic nuclei), star forming galaxies at $z=2-4$ have been detected and studied with imaging as well as spectroscopy (Steidel et al. 1996). These so called Lyman-Break Galaxies (LBGs) have star formation rates (SFRs) in the range $4-55h^{-2} M_{\odot} \text{ yr}^{-1}$ for $\Omega=1.0$ or $20-270 M_{\odot} \text{ yr}^{-1}$ for $\Omega=0.2$ (Pettini et al. 1998). Also, via the study of the class of high column density QSO absorption lines systems known as Damped Ly α Absorbers (DLAs) a wealth of information on the early chemical evolution of galaxies at $z=2-4$ has been obtained (e.g. Lu et al. 1996). The DLAs are in general forming stars at a significantly lower rate than the LBGs (Møller & Warren 1998, Fynbo et al. 1999).

Independent information about the formation of the brightest galaxies comes from detailed studies of the stellar populations of present day bright cluster ellipticals. These populations seems to have formed early ($z>2$) in strong burst of star formation (Bower et al. 1992). Studies of the fundamental plane for elliptical and lenticular galaxies in rich clusters at intermediate redshifts also indicate early formation times ($z>5$ for $\Omega=1$, Jørgensen et al. 1999), and the fundamental plane for field ellipticals at similar redshifts is consistent with being the same as in clusters (Treu et al. 1999a). Studies of the globular cluster populations of faint elliptical galaxies also indicate rather early formation times ($z>1$), whereas for bright cluster ellipticals the globular cluster populations do not strongly constrain the possible formation scenarios (Kissler-Patig et al. 1998). Furthermore, the presence of seemingly old stellar populations in elliptical galaxies at $z>1$ proves that at least some elliptical galaxies formed very early in strong bursts of star formation (Spinrad et al. 1997, Treu et al. 1999b, see also Jimenez et al. 1999). For first-rank ellipticals star formation rates as high as $\text{SFR} \sim 10^3 M_{\odot} \text{ yr}^{-1}$ would then be possible. A reason why such high star formation rates have not been detected in galaxies at high redshift may be that these galaxies are the hosts of powerful QSOs and hence are hidden by the light from the QSOs (e.g. Terlevich & Boyle 1993). Support for a connection between QSOs and bright elliptical galaxies comes from the fact that radio quiet QSOs as well as radio loud QSOs and radio galaxies at $z=0.1-0.3$ are hosted by galaxies for which the light profiles are best fit by de Vaucouleurs profiles indicating that they are early stages of massive ellipticals (McLure et al.

Send offprint requests to: J.U. Fynbo

^{*} Based on observations made with the Nordic Optical Telescope, operated on the island of La Palma jointly by Denmark, Finland, Iceland, Norway, and Sweden, in the Spanish Observatorio del Roque de los Muchachos of the Instituto de Astrofísica de Canarias.

Correspondence to: jfynbo@obs.aau.dk

Table 1. Observations of Q0151+048, Sept 17 – 20 and Oct 17 – 18, 1998

Filter	Combined seeing (arcsec)	Total integration (sec)
U	0.96	12500
B	0.84	24300
I	0.67	11750

1999). There is increasing evidence that QSOs at redshifts $z \approx 2$ are embedded in extended emission that is consistent with the presence of a stellar population in the QSO host galaxies. In the case of radio loud QSOs host galaxies have been detected in the optical and infrared by Lehnert et al. (1992) and Carballo et al. (1998), and in the case of radio quiet QSOs host galaxies have been detected in the optical and near infrared by Aretxaga et al. (1998a,b). There does not seem to be any systematic differences between the host galaxies of radio loud and radio quiet QSOs. Both populations of host galaxies are extremely bright, $R \approx 21-22$, and have optical-to-infrared colours in the range $R-K \approx 3-5$. However, measured polarisation of the light from some radio galaxies show that scattered QSO light can also contribute significantly to the observed extended emission (e.g. Cimatti et al. 1998).

In 1996 we performed a narrow band study of the $z_{abs} \approx z_{em}$ Damped Ly α Absorber (DLA, Wolfe et al. 1986) towards Q0151+048A using the 2.56-m Nordic Optical Telescope (NOT) (Fynbo et al. 1999). The main result of this study was the detection of extended Ly α emission from the DLA. The Ly α emission line had prior to this been detected in a spectroscopic study of Q0151+048A (Møller et al. 1998), but the large extended nature of the DLA absorber was quite unexpected. U band data, also from the 1996 run, hinted at the existence of an extended broad band object, but the signal-to-noise ratio of the object was low. We have therefore obtained deeper imaging of Q0151+048 in broad band U, B and I filters in order to confirm or reject our tentative detection, and to measure the extend and luminosity of the broad band source if real.

In Sect. 2 below we describe our new observations. In Sect. 3 we describe in detail the two independent methods we have used to search for extended objects close to the quasar. First we describe the image-deconvolution, where we used the Magain et al. (1998, hereafter MCS) algorithm, secondly we describe the direct PSF subtraction, and Sect. 4 we discuss our results.

In this paper we adopt $H=100 \text{ h km s}^{-1} \text{ Mpc}^{-1}$, $\Omega_m=1.0$ and $\Omega_\Lambda=0$ unless otherwise stated.

2. Observations and Data Reduction

The observations were performed during two observing runs in September and October 1998 with HiRAC (High Resolution Adaptive Camera) on the 2.56 m Nordic Optical Telescope. The CCD used was a 2048² back-side illuminated thinned Loral with a pixel size of 0.1082 arcsec.

Table 2. Measured sky level and rms of sky surface brightness.

passband	sky level	rms SB
	mag. arcsec ⁻²	mag. arcsec ⁻²
I(AB)	19.4	27.3
B(AB)	22.1	28.8
u(AB)	22.2	27.6

All 6 nights during which the observations were performed were photometric and with good seeing (median 0.7 arcsec FWHM in the I-band). Integration times in U were 1000-1500 sec in order to avoid the total noise to be dominated by read-out noise. In I and B the integration times were 250-300 sec and 300-500 sec respectively. Between exposures the telescope was moved 2-4 arcsec to minimize the effects of bad pixels and fringing. The total integration times in each filter are given in Table 1.

Also observed were several standard star sequences from Landolt (1992) and photometric solutions were obtained for each filter. For counts given as electrons per second we derive zero-points in the Landolt system of 22.77, 25.13 and 24.48 for u, B and I respectively. All magnitudes subsequently quoted in this paper are on the AB system. For the U-band we determined the colour equation $u = U + 0.17(U - B)$ relating the instrumental magnitude u to the standard Johnson U . There was substantial scatter around the fit near $U - B = 0$ of ~ 0.05 mag., which is typical for this band (e.g. Bessell 1990). The instrumental magnitudes u were converted to AB magnitudes using the equation $u(AB) = u + 0.58$, determined by integrating the spectrum of the star GD71 over the passband. Here we have retained the lower case u for the AB magnitude indicating that the effective wavelength of the filter lies significantly away from the standard value. The colour term for the I and B filters are consistent with zero i.e. $i = I$ and $b = B$, and we used the equations $I(AB) = I + 0.43$ and $B(AB) = B - 0.14$ (Fukugita et al. 1995) to put the I and B magnitudes onto the AB system.

The data were bias-subtracted, and twilight sky frames were used to flatten the frames in the standard way.

For the deconvolution, the individual bias subtracted and flattened I-band images were divided into six groups (chronologically) and the frames of each group were then combined using the optimal combination code described by Møller & Warren (1993), which maximizes the signal-to-noise ratio for faint sources. These six combined images were used in the simultaneous deconvolution process (see Sect. 3.1 below). Furthermore, all the individual I-band images were combined into one combined image, which was used in the PSF subtraction described in Sect. 3.2. In the same way we divided the individual bias subtracted and flattened B-band frames in four groups and calculated combined images for each group and for all images. Finally we combined the ten individual bias subtracted and flattened U-band frames into one combined image. The details of the sky noise in the combined images are provided in Table 2.

3. Analysis

3.1. Deconvolution

3.1.1. The deconvolution method

The images were deconvolved using the MCS algorithm. This method is based on the principle that the resolution of a deconvolved image must be compatible with its sampling, which is limited by the Nyquist frequency. The deconvolved image is decomposed into a sum of deconvolved point-sources plus a background smoothed on the length scale of the final resolution. The intensities and positions of the point-sources as well as an image of the more extended objects are given as output of the deconvolution procedure. Image decomposition allows objects blended with or even superposed on point-sources to be studied in some detail.

In order to check if the deconvolved model is compatible with the data, a residual map is computed. The residual map contains in each pixel the χ^2 of the fit of the model image (reconvolved with the PSF) to the original data of that pixel. The χ^2 image is used to determine the appropriate weight attributed to the smoothing of the image of extended sources in order to avoid under- or over-fitting of the data (see MCS for further details). A deconvolution compatible with the data should show a flat residual map with a mean value of 1 all over the image.

The MCS algorithm makes it possible to simultaneously deconvolve several frames. The advantage of this process is to derive the optimally constrained deconvolved frame which is simultaneously compatible with several different images of a given object. This results in a more accurate decomposition of the data than the deconvolution of one single combined frame. Moreover, applying the algorithm to many dithered frames leads to a deconvolved image with an improved sampling.

3.1.2. Application to the data

Simultaneous deconvolution of the U-band data from 1996 had already strongly indicated extended broad band emission in the direction of Q0151+048A (see Fig. 1). However, although the shape of the extended emission was similar to the one found in narrow-band (Fynbo et al. 1999), it was unclear to which extent systematic errors in the determination of the PSF influenced the detection and hence the signal-to-noise ratio of the object was too uncertain to constrain its morphology and luminosity.

There are two bright stars in the field of Q0151+048, referred to as psfA and psfB (see Fynbo et al. 1999). However, our new deep I-band data revealed that psfB has a faint red companion star at a projected distance of $0''.7$. In the I-band it is 4.3 magnitude fainter than psfB, in the B-band it is 6.3 magnitudes fainter than psfB, and in the U-band it remains undetected. In the following we only use psfA for the determination of the PSF.

We adopted for the deconvolved image a pixel size of $0''.0541$ (half of the original one), and a final resolution of 3 pixels FWHM, or $0''.16$ (the Nyquist limit is 2 pixels FWHM).

3.1.3. Results

Fig. 2 shows the deconvolved images in all three bands I, B and U. The images show the five sources already known to be in the field, namely the three point-sources qA, qB and the star s, and the two faint galaxies gA and gB south west of qA (see Fynbo et al. 1999 for details). However, there is also significant extended emission under the point-source emission from qA in all three bands. This emission have nearly identical morphology in the I and B bands with contours centred on the position of qA and with a slight elongation with position angle $\sim 20^\circ$ east of north. The shape and intensity of the extended U-band emission under qA (Fig. 2 right panel) is consistent with the shape and intensity derived from the 1996 U-band data (Fig. 1). Since the two sets of U-band data have been obtained with two different instruments, the consistency between the two measurements makes strong systematic errors unlikely. The morphology of the U-band emission is significantly more extended than the B and I morphology, about 4.5×2.2 arcsec², and has a position angle of about 100° east of north. This is very similar to that of the Ly α source S4, which extends over 6×3 arcsec² with position angle 98° east of north.

The extended emission towards qA is ~ 4 magnitudes fainter than that of the point-source emission. This high contrast makes it difficult to determine the exact ratio between the luminosity of the extended source (L_{Ext}) and that of qA (L_{QSO}). Several deconvolution solutions with different luminosity $L_{\text{QSO}}/L_{\text{Ext}}$ ratios are compatible with the residual map constructed as described above. Thus, there is some degeneracy between the plausible solutions found by the algorithm.

In order to demarcate the range of plausible solutions, a grid of 15 deconvolved images in each band was calculated, representing 5 different luminosity ratios $L_{\text{QSO}}/L_{\text{Ext}}$ and with 3 different values of the Lagrangian smoothing parameter applied during the deconvolution (see MCS for a description of the Lagrangian smoothing parameter). The solutions with the highest $L_{\text{QSO}}/L_{\text{Ext}}$ ratios were unphysical since they have a ring-shaped morphology, i.e. a hole at the position of the QSO. The lowest values of $L_{\text{QSO}}/L_{\text{Ext}}$ were rejected by inspection of the residual map mentioned above. The resulting range of magnitudes for the extended emission is given in Table 3. The solutions shown in Fig.2 are those with the highest acceptable values of $L_{\text{QSO}}/L_{\text{Ext}}$. Our conclusions concerning the morphology of the extended emission in the three bands are, however, unchanged for all solutions within the acceptable range.

In the B-band there is also significant extended emission under the PSF of the fainter neighbour quasar qB.

3.2. Object based image decomposition

In conclusion of the previous section: *i*) There is clear evidence for extended broad band (U, B and I) emission in the vicinity of the quasars Q0151+048A,B; *ii*) the morphology of the extended object(s) is identical in B and I but significantly different in U; *iii*) the U-band morphology is more extended and

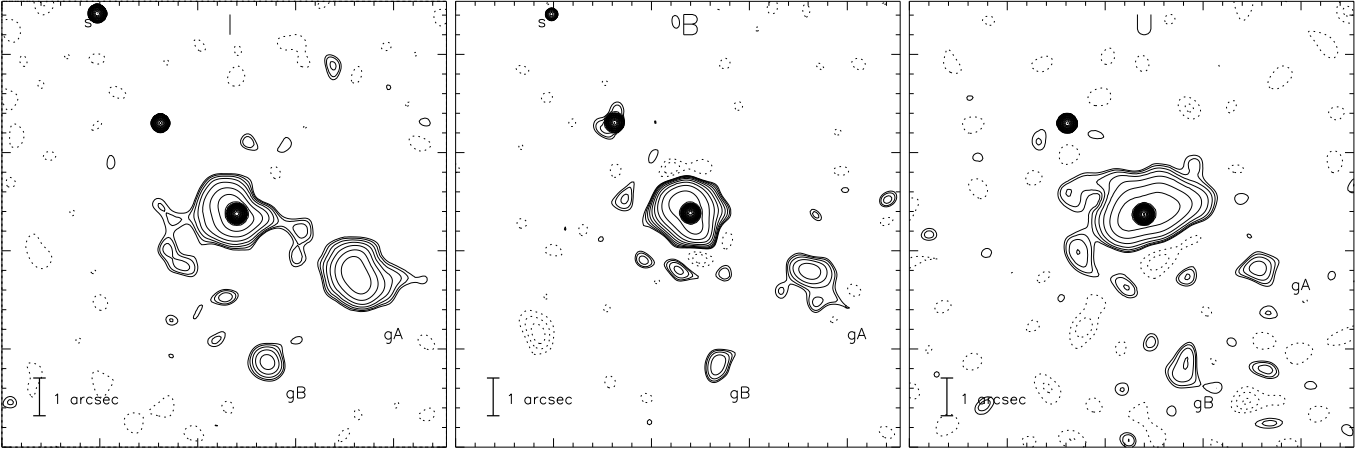


Fig. 2. Contour plots of 12×12 arcsec² surrounding the two QSOs from the deconvolved I-band frame (*left*), B-band frame (*middle*) and U-band frame (*right*). The three point-sources s, qB and qA are seen on the diagonal from the upper left corner (s) to the centre (qA). The resolution is $0''.16$. North is up and east to the left. Seen is the extended emission under qA and the two galaxies gA and gB south of qA.

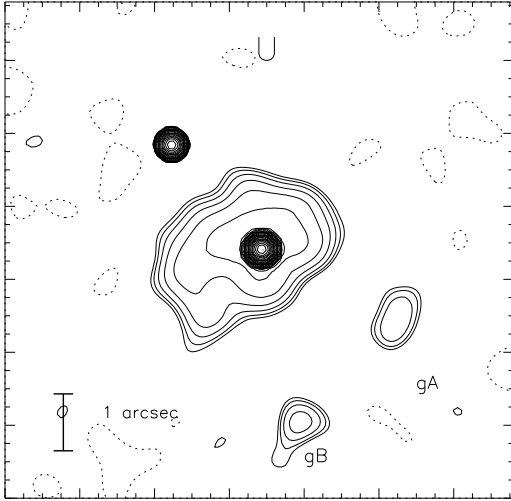


Fig. 1. Contours of the deconvolved U-band from 1996. The resolution is $0''.35$ and the axis are in units of arcsec. The contour levels are $-9, -6, -3, 3 \times 1\sigma$ of the sky noise and thereafter spaced logarithmically in factors of 1.5, with the dotted contours being negative. The field is 12×12 arcsec², North is up and East to the left.

similar to the morphology of the Ly α emission from the DLA absorbing galaxy (S4).

Those conclusions would suggest that the extended emission in this field is made up of three individual components: The DLA absorbing galaxy, the host galaxy of qA and the host galaxy of qB. The different morphology in the four different bands would then indicate that the objects have different spectral energy distributions (SEDs).

In order to investigate this further we decomposed the superimposed images into individual objects with different SEDs.

Table 3. Photometry of qA, qB and the extended sources under qA and qB. The magnitudes given for ExtA under Deconvolution is measured in a circular aperture with diameter 3.5 arcsec. The magnitudes for S4 and HGa under PSF-subtraction are determined by model fits as described in the text. The upper limits to the magnitudes of HGb are 2σ . The magnitudes of gA and gB are measured in a circular aperture with diameter 1.35 arcsec.)

	u(AB)	B(AB)	I(AB)
Deconvolution			
qA	17.81 ± 0.02	17.83 ± 0.02	17.46 ± 0.02
qB	21.00 ± 0.02	21.18 ± 0.02	20.69 ± 0.02
gA	23.85 ± 0.09	23.15 ± 0.02	21.77 ± 0.02
gB	24.02 ± 0.09	24.06 ± 0.02	23.18 ± 0.03
ExtA	21.8 – 21.3	21.3 – 20.7	21.8 – 21.2
NOT96			
ExtA	21.8 ± 0.2	-	-
gA	24.08 ± 0.06	-	21.87 ± 0.03
gB	24.18 ± 0.07	-	23.33 ± 0.05
PSF-subtraction			
HGa	21.7 ± 0.2	20.8 ± 0.2	21.5 ± 0.2
HGb	> 26.0	25.00 ± 0.10	> 25.7
S4	23.9 ± 0.3	24.1 ± 0.3	23.7 ± 0.3
gA	24.27 ± 0.12	23.51 ± 0.03	22.10 ± 0.03
gB	24.28 ± 0.12	24.53 ± 0.06	23.82 ± 0.09

For this image decomposition we applied the same procedure we used for the narrow band image analysis (Fynbo et al. 1999), but here we add more components. We consider point-sources, de Vaucouleurs profiles and exponential profiles. The best decomposition is determined as the minimum χ^2 fit following an iterative procedure as described below.

3.2.1. B-band data

The B-band image is more than a magnitude deeper than the I and U-band images in terms of the background rms surface brightness. Our first step was therefore to produce optimized models of the galaxies from the B-band data. For the decomposition we considered the following 8 components: Three point-sources (qA, qB, s), four galaxies to be fitted (gA, gB and the host galaxies of qA and qB, in what follows named HGa and HGb), and one galaxy of “frozen” morphology (the DLA absorbing galaxy S4). For S4 we adopted the model determined from the narrow-band data (Fynbo et al. 1999). Note that most of the objects do not overlap significantly, thus allowing us to fit them independently.

The bright star psfA was used with DAOPHOT II (Stetson 1997) to define the PSF. We then employed the iterative χ^2 minimization procedure detailed in Fynbo et al. 1999, to decompose the image of qA into a point-source and a de Vaucouleurs galaxy model (convolved with the PSF). For the calculation of the χ^2 we excluded a circular region of radius 0.65 arcsec centred on qA due to the large PSF-subtraction residuals. After ten iterations a stable solution was found. The same procedure repeated with an exponential-disc profile instead of the de Vaucouleurs profile resulted in a much poorer fit. A significant positive residual, centred about 1 arcsec east of qA, was left after this procedure. The most plausible interpretation of the residual is that it originates from the DLA absorbing galaxy S4. As S4 is known to extend across the position of the bright quasar, measuring its flux from a direct aperture measurement is impossible because of the large PSF subtraction residuals. Instead we made a grid of models to determine the flux of S4 via minimum χ^2 fitting. For a given assumed B magnitude of S4 we first subtracted the correctly scaled exponential-disc model as determined from the original Ly α image (Fynbo et al. 1999). For that given B magnitude of S4 we then repeated the iterative fitting of a de Vaucouleurs profile to the remaining flux. The final model was chosen to be the model with the smallest χ^2 measured in an area excluding pixels less than 0.65 arcsec from qA. The improvement in the fit due to the inclusion of the S4 model was significant ($\Delta\chi^2 = -21$). We also fitted the profiles of the two galaxies gA and gB. For gA the best fit was obtained with an exponential-disc profile, whereas the best fit for gB was obtained with a de Vaucouleurs profile.

Fig. 3b shows a 14×14 arcsec² field of the area after subtraction of the qA and qB PSFs as determined from the minimum χ^2 fit. The residuals, after the additional subtraction of the final models for HGa, gA and gB can be seen directly below (Fig. 3e). The magnitude of HGb was measured on this final subtracted image.

3.2.2. U and I band data

The well constrained galaxy models determined from the high signal-to-noise B image were subsequently used to decompose the U and I-band data. Since the combined seeing of the U-band data was poorer than that of the B image, we first

smoothed the galaxy models to the seeing of the U-band data. For a large grid of U-band magnitudes of S4 and HGa we then subtracted scaled versions of the smoothed S4 and HGa galaxy models, fitted and subtracted the quasar point source component using DAOPHOT II, and finally calculated the χ^2 in an area excluding pixels less than 0.8 arcsec from qA. The final model was selected to be that which had the smallest χ^2 . The U magnitudes of the galaxies gA and gB were determined in the same way. For the decomposition of the combined I-band data, which have a better seeing than the B-band data, we first smoothed the I-band image to the seeing of the B image and then proceeded as for the U-band data.

Results of this procedure can be seen in Fig. 3a,d and Fig. 3c,f for the I and U-bands respectively. As for the B-band data the upper frames show the fields after subtraction of final fits of qA and qB only, while in the lower frames the fitted models of galaxies HGa, gA and gB have also been subtracted. The magnitudes (and estimated associated errors) of objects resulting from the fitting procedure are listed in Table 3.

4. Summary and discussion

Our original interest in the field of Q0151+048A was to identify the DLA galaxy in front of it. This identification was accomplished via imaging in Ly α (Fynbo et al. 1999), but our broad band images left some questions open. The purpose of the deeper broad-band data presented in this paper was to clarify this situation. We shall here first summarise our findings, then briefly consider their implications.

4.1. Results summary

Our new data have unambiguously confirmed the presence of extended emission in the field in all three bands I, B and U. The different morphology seen in the three bands strongly suggest that we see three objects superimposed: The quasar, the DLA absorbing galaxy and the quasar host galaxy.

The superposition of three close objects of widely differing brightnesses causes considerable degeneracy for any attempt to determine the brightness of the faintest sources, and it is therefore impossible to find a unique solution for the flux of the faintest object (the DLA galaxy S4). Nevertheless, we find that S4 is clearly detected in the U image. The U-band magnitude of S4 determined via our minimum χ^2 procedure is fully consistent (to within 1σ) with being caused by the known Ly α flux at 3565Å alone. The data are therefore consistent with a zero contribution from any continuum source in the U-band.

It is difficult to determine the exact errors on the I and B magnitudes of S4, but for both images we found a very significant improvement in the reduced χ^2 of the fit when we included S4. It is therefore likely that S4 is indeed a low surface brightness continuum source, but this question is going to be extremely hard to settle.

The existence of a separate extended continuum source centred on qA is, however, clearly demonstrated independently in

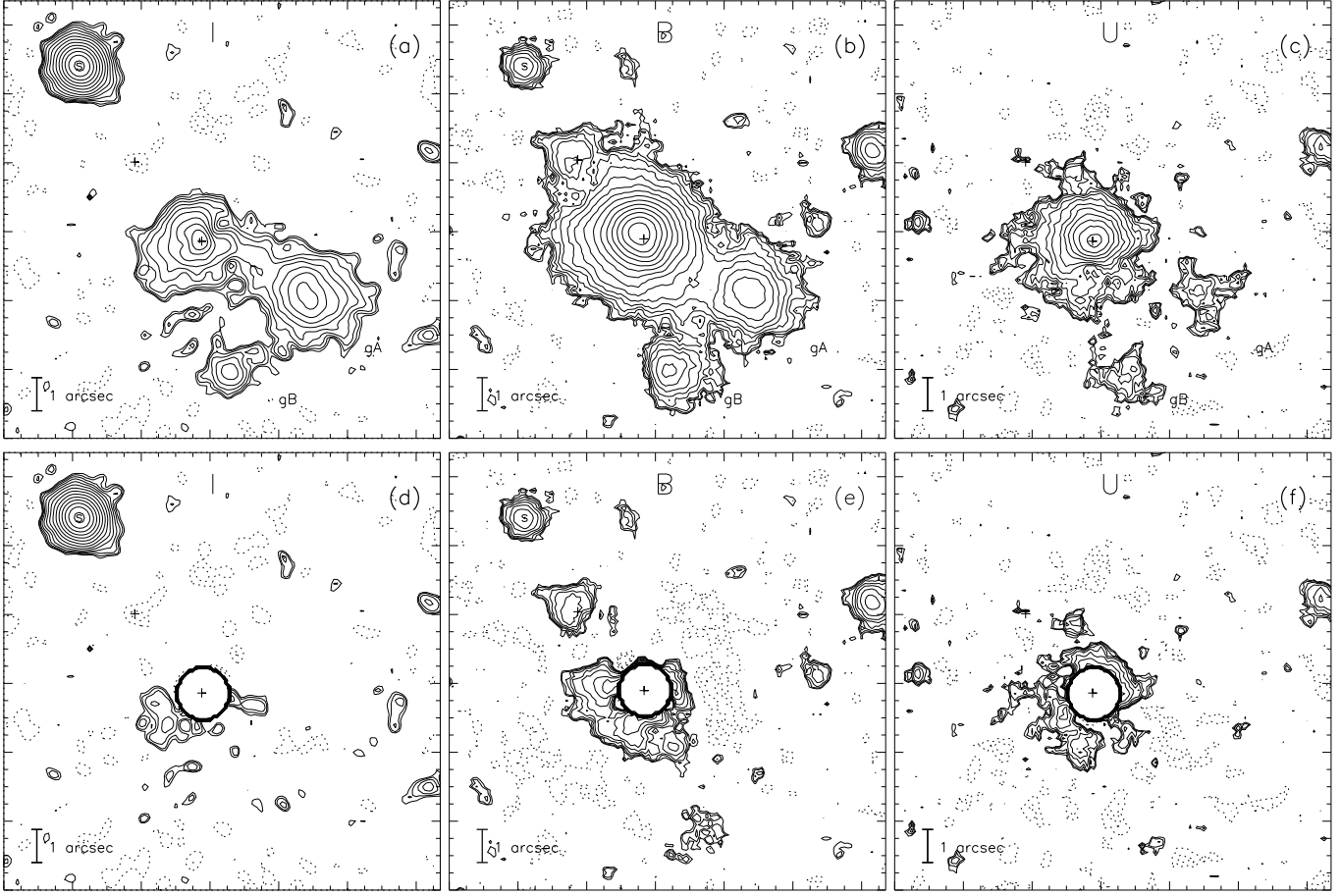


Fig. 3. Contour plots of $14 \times 14 \text{ arcsec}^2$ surrounding the two QSOs from the final combined and PSF subtracted frames in a) I-band, b) B-band and c) U-band. North is up and east to the left. Seen is residual extended emission under qA. Also seen are the two galaxies gA and gB south of qA. The contour levels are $-9, -6, -3, 3 \times 1\sigma$ of the sky noise and thereafter spaced logarithmically in factors of 1.5, with the dotted contours being negative. d) – f) show the same region after subtraction of the galaxy fits of HGA, gA and gB as described in the text.

The most plausible explanation for the residual east of the position of qA is the absorber galaxy S4.

all bands. This result was arrived at independently via image deconvolution, and via our iterative object fitting technique.

4.2. Discussion: Starburst Galaxy or Dust scattering

The distance modulus (for $z=1.93$) in the assumed cosmology with $h=0.5$ is 45.8. Assuming instead $\Omega=0.3$ and $\Omega_\Lambda=0.7$ the corresponding distance modulus becomes 46.6. Hence, the absolute AB magnitudes of the host galaxy HGA is $<-24.0(-24.8)$ in U (rest frame 1100–1300Å), $<-24.5(-25.3)$ in B (rest frame 1300–1500Å) and $<-24.0(-24.8)$ in I (rest frame 2300–3400Å). Such extremely bright magnitudes are in the local universe only connected with brightest cluster galaxies (for comparison M87 and Centaurus A both have absolute magnitudes of roughly -23 in the V-band). Brightest cluster members can be as bright as -26 (Oemler 1976). Interestingly we find that the absolute magnitude of HGA is similar to those of the extended ‘fuzz’ that have been detected around other high redshift QSOs by

Lehnert et al. (1992), Carballo et al. (1998) and Aretxaga et al. (1998a,b).

The morphology of the host galaxy HGA is best fit by a de Vaucouleurs profile. The fit to an exponential-disc leads to a much poorer fit. A plausible interpretation of the data is therefore that we see the early stage of a massive elliptical galaxy in the process of forming the bulk of its stars. Assuming that all the light is coming from stars, and not e.g. scattered quasar light (see below), we can estimate the star formation rate (SFR) needed to explain the observed fluxes. In the case of continuous star formation we can adopt the relation between the SFR and the luminosity at 1500Å $\text{SFR} = L_{1500} / (1.3 \times 10^{40} \text{ erg s}^{-1} \text{ \AA}^{-1})$ commonly used for LBGs (Pettini et al. 1998) and we hence infer a star formation rate of order $100(200) M_\odot \text{ yr}^{-1}$ for $\Omega=1(0.3)$ and $\Omega_\Lambda=0(0.7)$. For instantaneous bursts we can use the Starburst99 package (Leitherer et al. 1999) to infer the colours of models calculated with solar metallicity and ages 1, 10 and 100 million years. The colours for these three models are given in Table 4.

Table 4. The colours of instantaneous starbursts with four different ages. The colours of HGa are listed for comparison.

Age (Myr)	u-B	B-I
1	-0.2	-0.7
10	-0.1	-0.3
100	0.7	0.3
Exta	0.0–1.1	-1.1–0.1
HGa	0.9 ± 0.3	-0.7 ± 0.3

The colours of the host, $0 < u-B < 1.1$, $-1.1 < B-I < 0.1$ from Deconvolution and 0.9 ± 0.3 , -0.7 ± 0.3 from PSF-subtraction, are roughly consistent with instantaneous bursts with ages in the range 10–100 Myr. The number of stars formed in the burst would be in the range from 10^8 to a few times 10^9 stars depending on the age of the burst and on the assumed cosmology.

Another interpretation of the extended fuzz frequently seen around quasars, is light from the quasar itself scattered by dust. This mechanism is well known from radio galaxies at high redshifts where scattering off dust grains has revealed the existence of “hidden” quasars in the galaxy cores. It is likely that radio quiet QSOs have similar non-isotropic radiation fields (see e.g. the discussion in Møller & Kjærgaard 1992), and in that case our line of sight is such that we look straight down the emission cone inside of which the scattering is taking place. In this case we therefore expect to see the quasar emission cone “end on” via forward scattered quasar light. The scattering process is expected to be essentially grey and recent calculations predict that as much as 10% of the quasar light could be scattered in this way (Witt & Gordon, 1999; Városi & Dwek, 1999; Vernet et al. in prep.). If considering a clumpy medium, we would expect dust scattered light to be emitted from inside a very large volume in front of the quasar. When taking the cone geometry into account one would expect its total flux to be roughly a few % of the quasar flux at any given wavelength (Fosbury, private communication). From Table 3 we find that the flux from HGa is 3, 6 and 2% of the flux from Q0151+048A in U, B and I respectively. Similar, but less significant, results are found for HGb. It is not yet known if the light profile of scattered light from a cone will reproduce a de Vaucouleurs profile, but since this seems to be a universally preferred profile it is not unlikely. One thing worth noting in Fig. 3e are the negative residuals surrounding the position of qA at a distance of 2–3 arcsec after subtraction of the fitted de Vaucouleurs profile. This indicates that the true profile of HGa in reality falls off steeper than a de Vaucouleurs profile. If model calculations were to show such a steep profile for forward scattered light in a radiation cone, that would be a strong hint towards the nature of the quasar fuzz.

However, the colours of the extended emission as seen in Table 3 and Fig. 4 are significantly different from those of the two QSOs, which argues against the scattering hypothesis. Hence, we conclude that at least a significant fraction of the observed extended emission must be caused by a star burst.

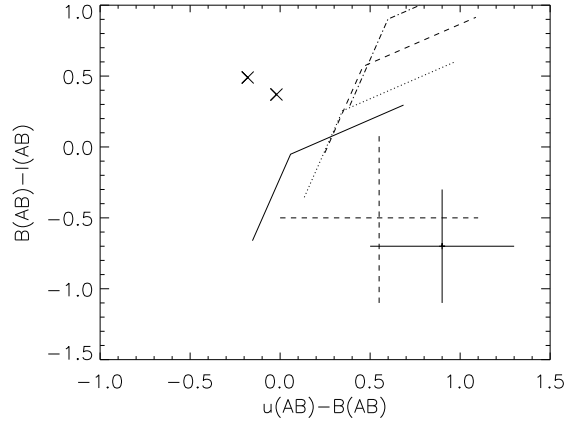


Fig. 4. The $B(AB)-I(AB)$ vs. $u(AB)-B(AB)$ colours of qA and qB (marked by \times), of the instantaneous star burst models of Table 4 (thick, full drawn line). The dotted, dashed and long dashed lines show the colours of reddened bursts assuming $A(B_{Rest})=0.5$ and MW, LMC and SMC extinction curves respectively. The colours of the extended emission under qA is marked by the error-bars. The dashed error-bar represents the measurement from deconvolution and the full drawn error-bar the measurement from PSF-subtraction.

Acknowledgments

We wish to thank Pierre Magain and Peter Stetson for making available the MCS-code and DAOHPOT-II respectively. We have benefitted from stimulating discussions with R. Fosbury and J. Vernet on the subject of dust scattering, and with C. Jean on the subject of reddening models of galaxy spectra. We thank the anonymous referee for valuable comments that clarified the paper on essential points. JUF thanks the European Southern Observatory for support from the ESO studentship programme. IB thanks the European Southern Observatory for support from the ESO visitor programme. IB was supported in part by contract ARC94/99-178 “Action de Recherche Concertée de la Communauté Française (Belgium)” and Pôle d’Attraction Interuniversitaire, P4/05 (SSTC, Belgium).

References

- Aretxaga I., Terlevich R.J., Boyle B.J., 1998a, MNRAS 296, 643
- Aretxaga I., Le Mignant D., Melnick J., Terlevich R.J., Boyle B.J., 1998b, MNRAS 298, L13
- Bessell M. S., 1990, PASP 281, 817
- Bower R.G., Lucey J.R., Ellis R.S., 1992, MNRAS 254, 601
- Carballo R., Sánchez S.F., González-Serrano J.I., Benn C.R., Vigotti M., 1998, AJ 115, 1234
- Cimatti A., di Serego Alighieri S., Vernet J., Cohen M., Fosbury R.A.E., 1998, ApJ 499, L21
- Forbes D.A., Brodie J.P., Grillmair C.J., 1997, AJ 113, 1652
- Fukugita M., Shimasaku K., Ichikawa T., 1995, PASP 107, 945
- Fynbo J.U., Møller P., Warren S.J., 1999, MNRAS 305, 849
- Jimenez R., Friaca A.C.S., Dunlop J.S., et al., 1999, MNRAS 305, L16

- Jørgensen I., Franx M., Hjorth J., Van Dokkum P., 1999, MNRAS 308, 833
- Kissler-Patig M., Forbes D.A., Minniti D., 1998, MNRAS 298, 1123
- Landolt A.U., 1992, AJ 104, 340
- Lehnert M. D., Heckman T.M., Chambers K.C., Miley G.K., 1992, ApJ 393, 68
- Leitherer C., Schaerer D., Goldader J.D., et al., 1999, ApJS 123, 3
- Lu L., Sargent W.L.W., Barlow T.A., Churchill C.W., Vogt S.S., 1996, ApJS 107, 475
- Magain P., Courbin F., Sohy S., 1998, ApJ 494, 472
- McLure R.J., Kukula M.J., Dunlop J.S., et al., 1999, MNRAS 308, 377
- Møller P., Kjærgaard P., 1992, A&A 258, 234
- Møller P., Warren S.J., 1993, A&A 270, 43
- Møller P., Warren S., 1998, MNRAS 299, 661
- Møller P., Warren S., Fynbo J.U., 1998, A&A 330, 19
- Pettini M., Kellogg M., Steidel C.C., et al., 1998, ApJ 508, 539
- Spinrad H., Dey A., Stern D., et al., 1997, ApJ 484, 581
- Steidel C.C., Giavalisco M., Pettini M., Dickenson M., Adelberger K.L., 1996, ApJ 462, L17
- Stetson P., 1997, "User's Manual for DAOPHOT II"
- Terlevich R.J., Boyle B.J., 1993, MNRAS 262, 491
- Treu, T., Stiavelli, M., Casertano, S., Møller, P., Bertin, G., 1999a, MNRAS 308, 1037
- Treu T., Stiavelli M., Walker A.R., et al., 1999b, A&A 340, L10
- Oemler, 1976, ApJ 209, 693
- Városi F., Dwek E., 1999, ApJ 523, 265
- Witt A.N., Gordon K.D., 1999, ApJ, in press
- Wolfe A.M., Turnshek D.A., Smith H.E., Cohen R.D., 1986, ApJS 61, 249